Crystallization induces thermally activated delayed fluorescence of Ag_{14} nanocluster†

Jin-Sen Yang,[a] Lu-Yao Xiao,[b] Fan Liu,[b] Jun Xu,[a] Xi-Yan Dong,*[ab] Jia-Hua Hu,*[b] Jing Li*[c] and Shuang-Quan Zang[b]

[a.] *College of Chemistry and Chemical Engineering, Henan Polytechnic University, 454000 Jiaozuo (China)*

[b.] *College of Chemistry, Zhengzhou University, 450001 Zhengzhou (China)*

[c.] *School of Science, Xuchang University, 461000, Xuchang, (China)*

Contents

Materials and reagents

4,5-dicyanobenzene-1,2-dithiolate (dcbdt) was synthesized following a literature method.[1] All other chemicals and solvents used were of commercially available reagent grade and were used without further purification. All solvents were of analytical grade reagent.

The synthesis of Ag_{14}-dcbdt

Silver trifluoroacetate (11 mg, 0.05 mM), tri-p-tolylphosphane (18 mg, 0.06 mM), dcbdt (4 mg, 0.02 mM) and tetraoctylammonium nitrate (11 mg, 0.02 mM) was dissolved in a mixed solution of dichloromethane (3 mL) and acetonitrile (3 mL), then 1 mL of ethanol containing 2 mg (0.02 mM) borane tert-butylamine complex was added. After being stirred for approximately 10 min at room temperature, the orange-red solution was kept in the dark for 1 day to yield red rhombic crystals. Yields: 35% based on the dcbdt ligand.

Instrumentation and characterization

X-ray photoelectron spectroscopy (XPS) was measured on Thermo Scientific ESCALAB 250Xi spectrometer equipped with a 300 W aluminum target radiation source (Al Kα). Powder X-ray diffraction patterns (PXRD) were collected on a Rigaku MiniFlex 600 diffractometer with CuKa radiation (λ = 1.5418 Å) at 30 kV. UV-vis-NIR absorption spectra were recorded using a Hitachi UH4150 UV-Visible spectrophotometer in the range 300-1500 nm. UV-visible diffuse reflectance spectra of samples were recorded in the range of 250-700 nm using a UH4150 spectrophotometer equipped with an integrating sphere. Steady-and transient-state photoluminescence (PL) spectra were record with a HORIBA FluoroLog-3 fluorescence spectrometer. Fourier transform infrared (FT-IR) spectra were recorded on a Bruker ALPHA II spectrometer. Full-time domain fluorescence lifetime data acquisition using M-X355L picosecond laser in combination with FF4 fluorescence lifetime decoder (Orient KOJI Ltd, Tianjin CHN), The detector use PPD850 photon counting detector (TTS 180ps, Horiba JobinYvon IBH, UK).

X-ray Crystallography

Single-crystal X-ray diffraction measurements of Ag_{14}-dcbdt, were performed on a Rigaku XtaLAB Pro diffractometer with Cu-K_α radiation (λ = 1.54178 Å) at 200 K, respectively. Data collection and reduction were performed using the program CrysAlisPro[2]. The two structures were all solved with direct methods (SHELXS)[3] and refined using full-matrix least-squares based on F^2 with the programs SHELXS-97 and SHELXL-97 within OLEX2.[4-5] All the atoms were refined anisotropically with the exception of some solvent molecules and hydrogen atoms were placed in calculated positions refined using idealized geometries and assigned fixed isotropic displacement parameters. Structure refinement was operated with different restraints and constraints (ISOR, SIMU, DFIX) in the corresponding crystallographic CIF files. The SQUEEZE routine in the PLATON software was applied to subtract the diffraction contribution from the disordered solvent molecules in the structures. The detailed information of the crystal data, data collection and refinement results for all complexes are summarized in Tables S1.

Transient absorption (TA) measurement

The transient absorption spectra were recorded on a commercial pump-probe system with microscope (Helios-EOS, Ultrafast Systems LLC) in combination with a femtosecond laser system (Astrella, Coherent). Laser pulses (800 nm center wavelength, 100 fs duration, 1 kHz repetition rate, 7 mJ/pulse) were generated by a Ti:Sapphire-based regenerative amplified laser system. The laser pulses were spilt to generate pump and probe beam. The pump pulses at 300 nm were delivered by an optical parametric amplifier which was excited by a portion of 800 nm laser pulses. For femtosecond transient absorptions in CH_2Cl_2 solution, the pump pulse energy was 50 $\mu J/cm^2$ at the sample cell. The probe and reference beams were generated by focusing the 800 nm beam (split from the amplifier with a tiny portion) to a sapphire crystal. The pump-probe delay was controlled by an optical delay line. The pump-probe delay time was electronically controlled. TA signal was obtained by detecting the intensity of probe and reference pulses with and without pumped light, and global analysis was performed by Glotaran software.

Femtosecond transient absorptions of Ag_{14}-dcbdt crystal are measured by the single crystal microimaging detection system, and the specific position of a single crystal is measured by a long working distance 50× objective lens. The camera provides a direct enlarged view of the sample. The probe beam was generated by focusing the 800 nm beam to another sapphire crystal. The pump pulse at 400 nm with an energy of 450 $\mu J/cm^2$. The pump-probe delay also was controlled by the same optical delay line. TA signal is obtained by detecting the intensity of probe light with and without pumped light, and global analysis is performed by Glotaran software.

Density functional theory (DFT) calculations

The density functional theory (DFT) and time-dependent density functional theory (TD-DFT) calculation were performed with Gaussian 16[6] under Perdew-Burke-Ernzerhof (PBE0) functional.[7] All calculations were performed using 6-31g* basis set for H, C, N, P and S atoms,[8-9] and Lanl2DZ effective core potentials for Ag atom.[10-12] The solvation effects were incorporated into the quantum mechanical calculations using the Conductor-like Polarizable Continuum Model (CPCM) with dichloromethane as the solvent. The self-consistent reaction field (SCRF) method was employed to account for the solvent environment during the optimization and electronic property calculations. The theoretical UV-Vis spectra were calculated using TD-DFT and plotted based on the computation of the lowest 200 singlet-to-singlet excitation energies.

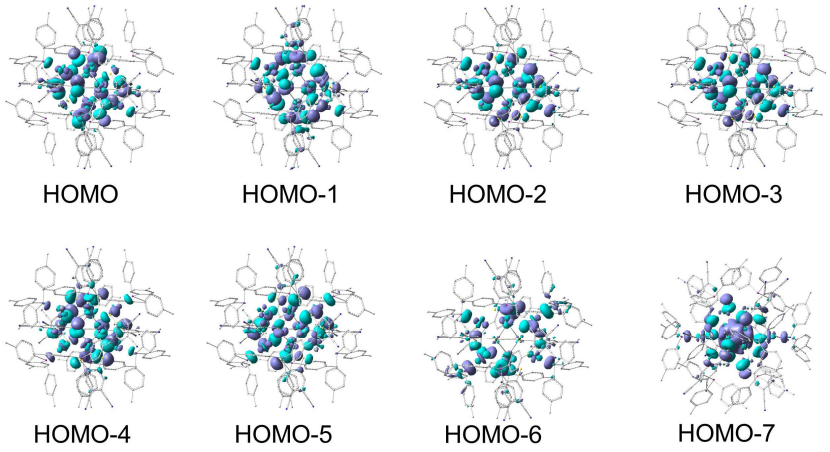

Figure S1. Selected representations of frontier occupied molecular orbitals for Ag_{14}-dcbdt (isovalue = 0.02).

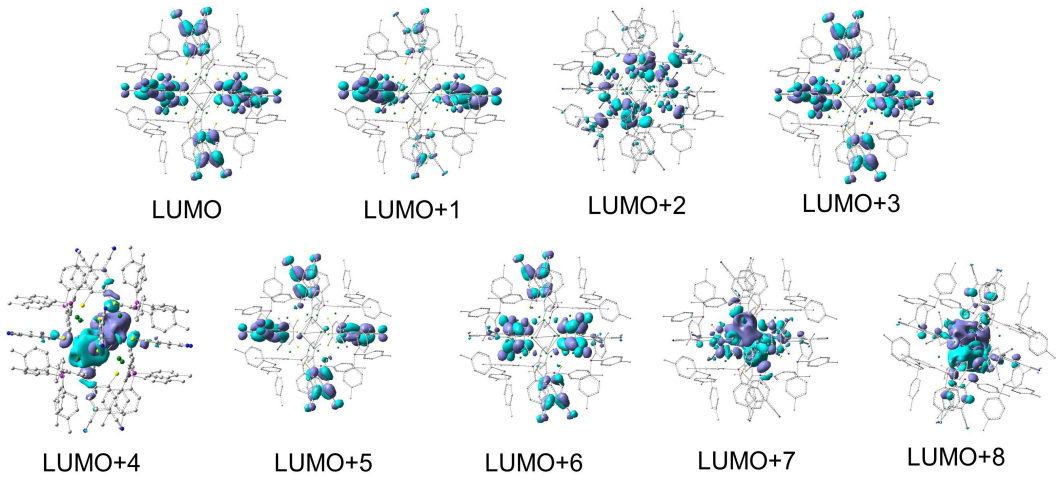

Figure S2. Selected representations of frontier unoccupied molecular orbitals for Ag_{14}-dcbdt (isovalue = 0.02).

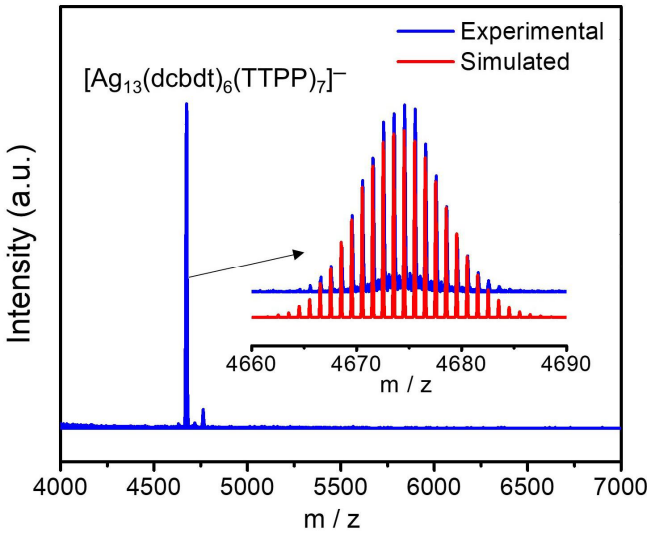

Figure S3. Negative-ion ESI-MS of Ag_{14}-dcbdt in CH_2Cl_2.

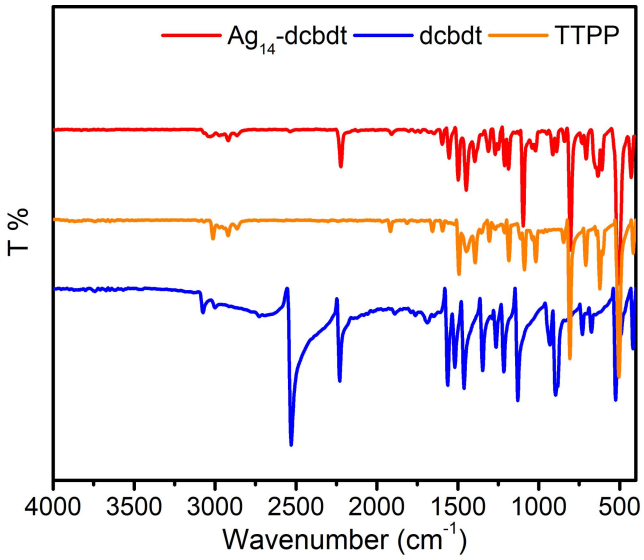

Figure S4. FT-IR spectra of Ag_{14}-dcbdt, dcbdt and TTPP ligands.

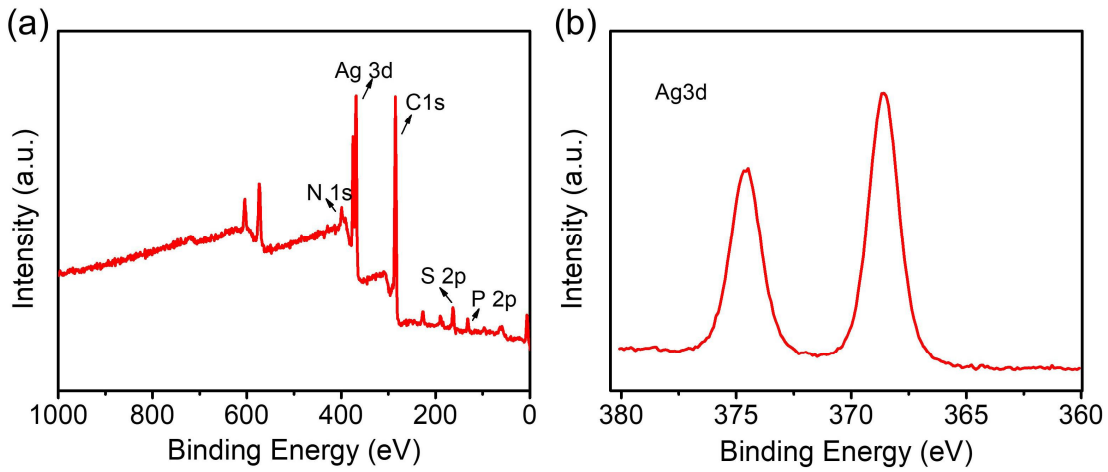

Figure S5. (a) The survey scans XPS profiles of Ag_{14}-dcbdt. (b) High resolution XPS for Ag 3p of Ag_{14}-dcbdt.

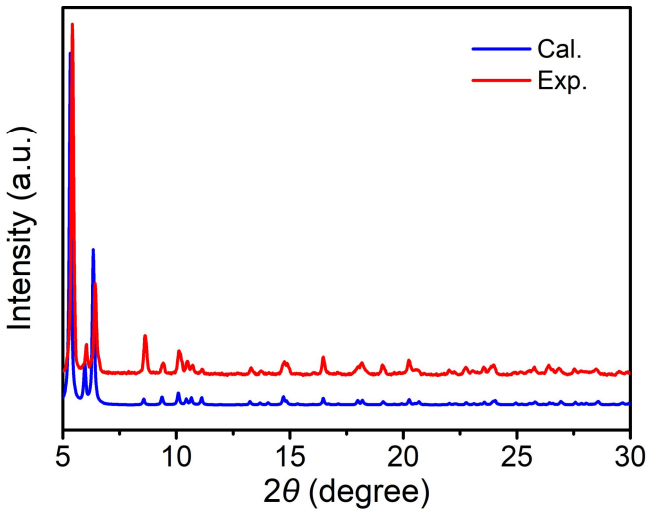

Figure S6. The experimental and simulated PXRD patterns of Ag_{14}-dcbdt.

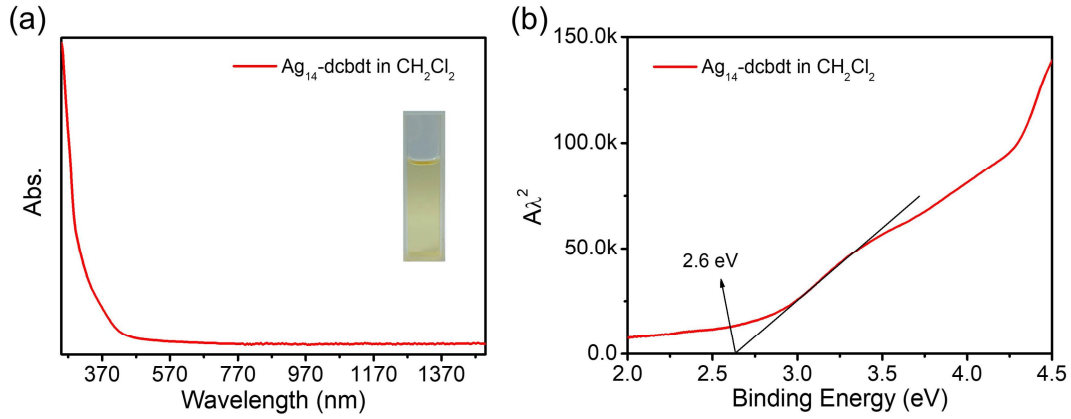

Figure 7. (a) The optical absorption spectrum of Ag_{14}-dcbdt. Inset: A photo of Ag_{14}-dcbdt in CH_2Cl_2. (b) The optical bandgap of Ag_{14}-dcbdt in CH_2Cl_2.

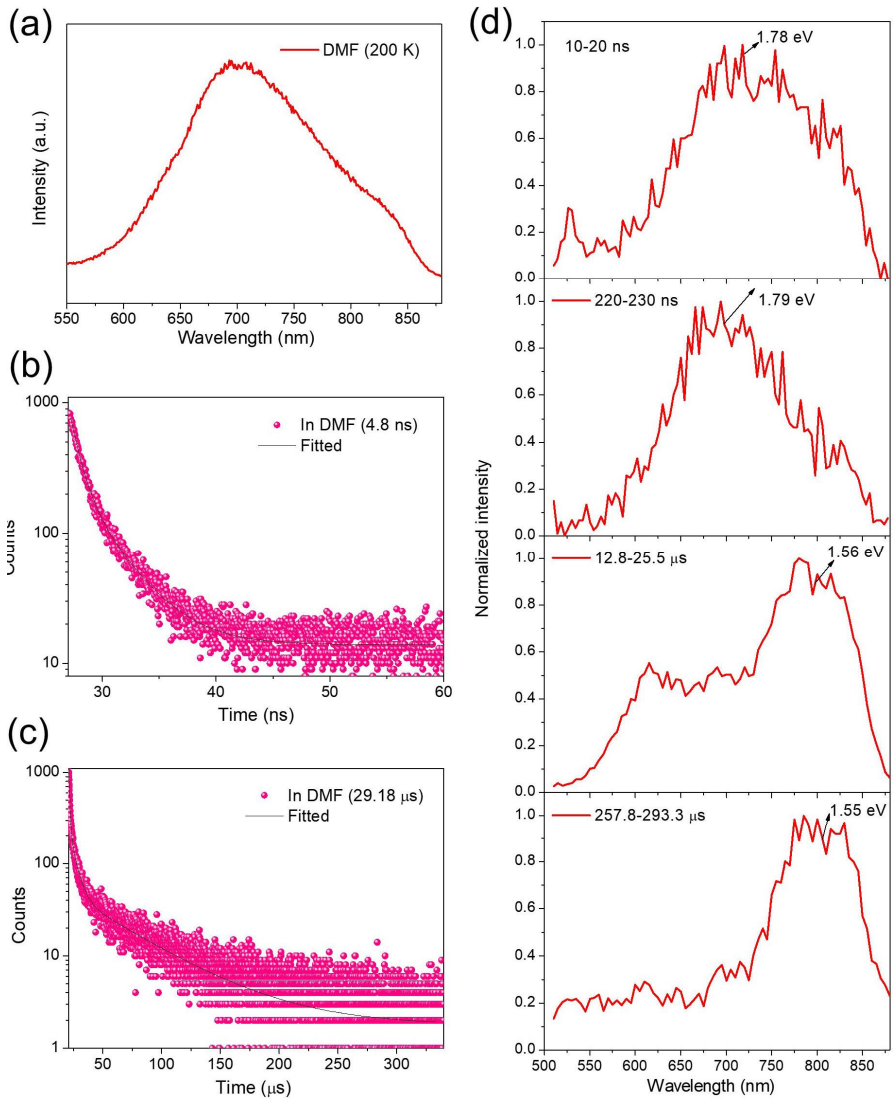

Figure 8. PL properties of Ag_{14}-dcbdt in DMF at 200 K. (a) PL emission spectra. (b) PL decay spectrum excited by a 370 nm nanosecond laser. (c) PL decay spectrum at 696 nm excited by a 355 nm microsecond laser. (d) PL spectra on different time scales.

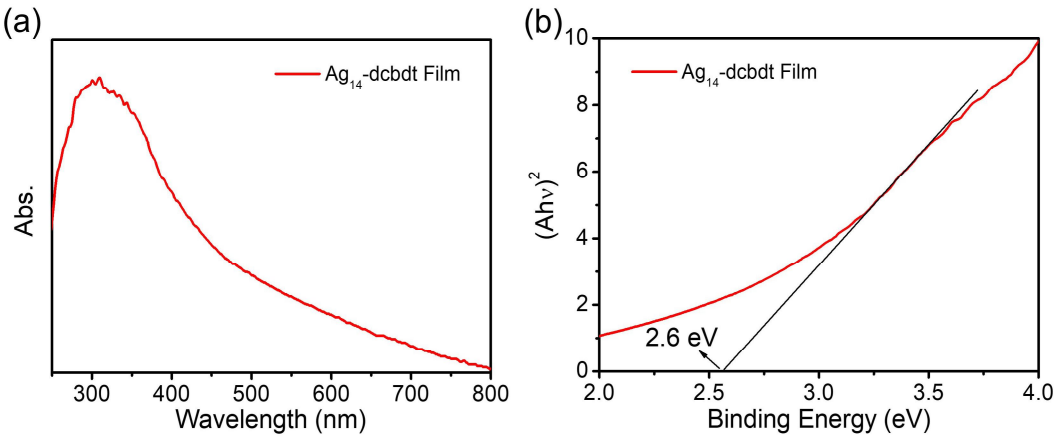

Figure S9. (a) The UV-visible diffuse reflectance spectrum of Ag_{14}-dcbdt PMMA film. (b) The optical bandgap of Ag_{14}-dcbdt PMMA film.

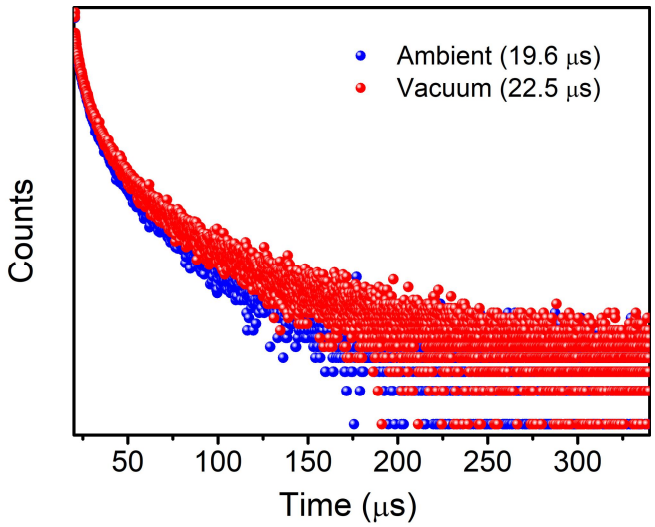

Figure S10. PL decay spectra at 665 nm of Ag_{14}-dcbdt PMMA film under ambient and vacuum conditions (Excited by a 355 nm microsecond laser).

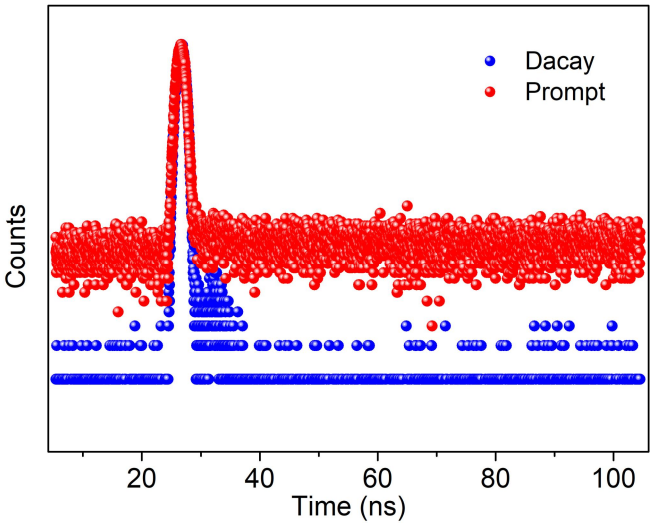

Figure S11. PL decay spectrum of Ag_{14}-dcbdt PMMA film at 665 nm (Excited by a 370 nm nanosecond laser).

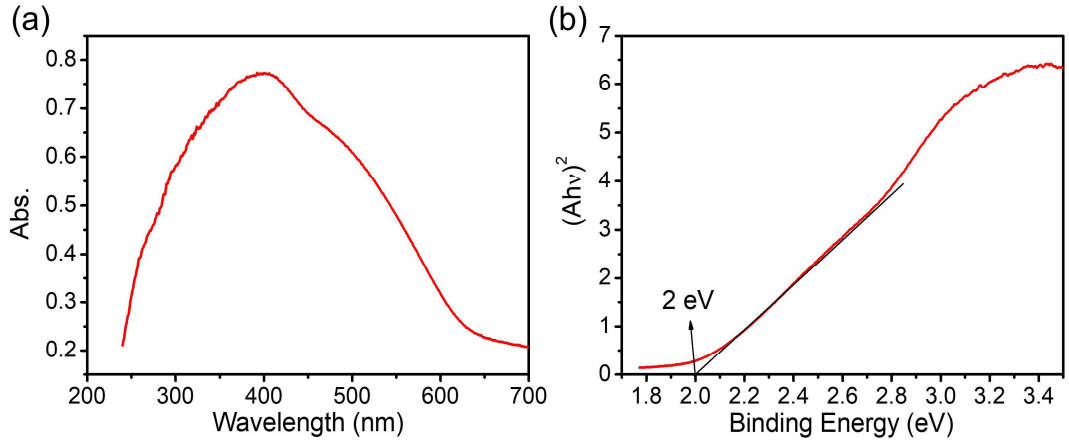

Figure S12. (a) The UV-visible diffuse reflectance spectrum of crystalline Ag_{14}-dcbdt. (b) The optical bandgap of crystalline Ag_{14}-dcbdt.

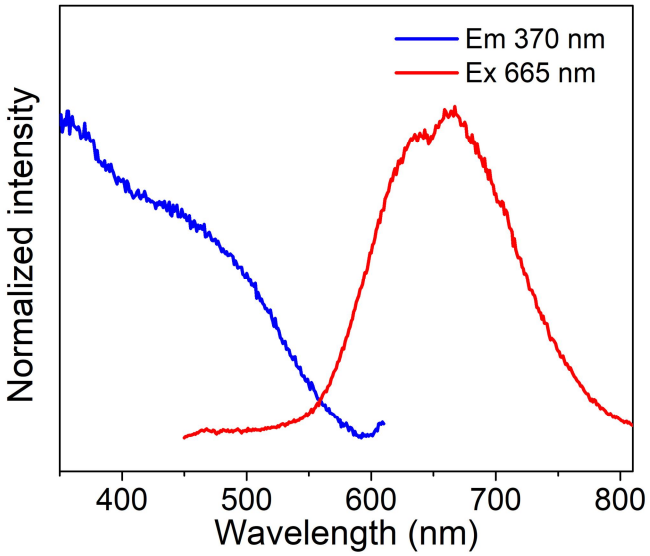

Figure S13. Excitation and emission spectra of Ag_{14}-dcbdt crystals.

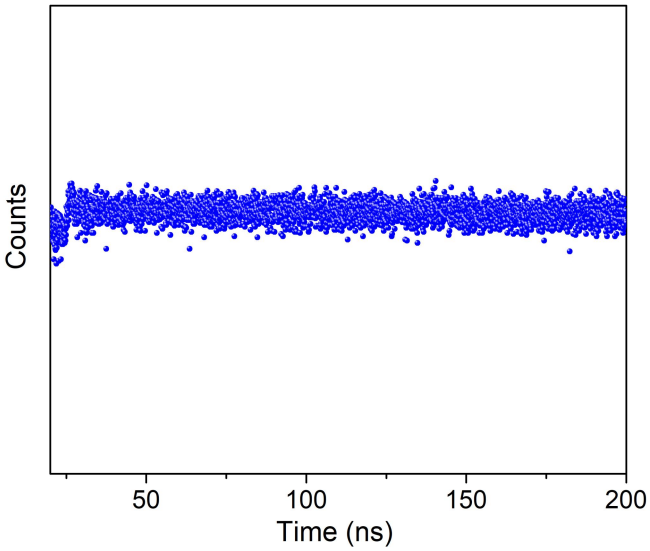

Figure S14. PL decay spectrum at 665 nm of Ag_{14}-dcbdt crystals (Excited by a 370 nm nanosecond laser).

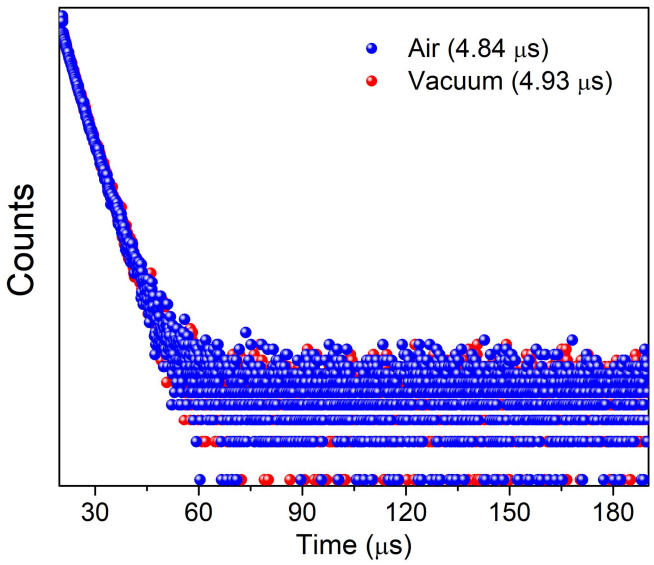

Figure S15. PL decay spectra at 665 nm of Ag_{14}-dcbdt crystals under ambient and vacuum conditions (Excited by a 355 nm microsecond laser).

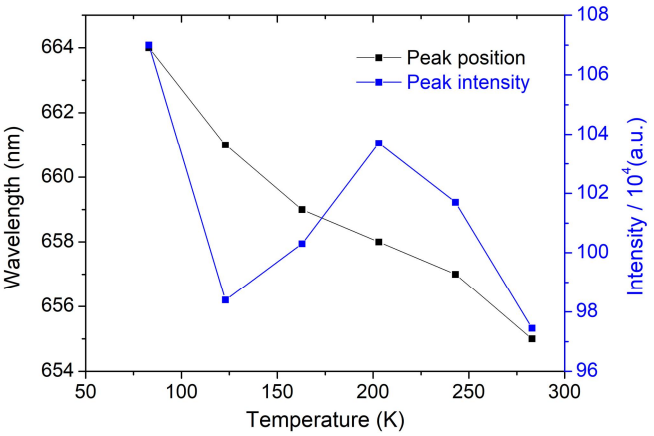

Figure S16. The emission intensity and position of temperature-dependent Ag_{14}-dcbdt crystals in the range of 83 to 283 K.

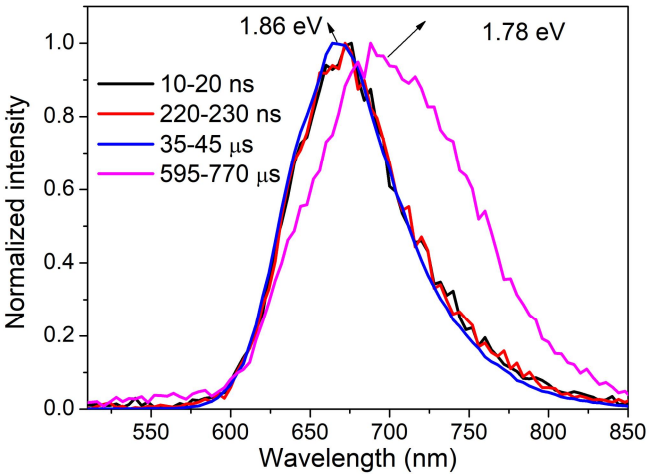

Figure S17. PL spectra of crystalline samples of Ag_{14}-dcbdt at 83 K on different time scales.

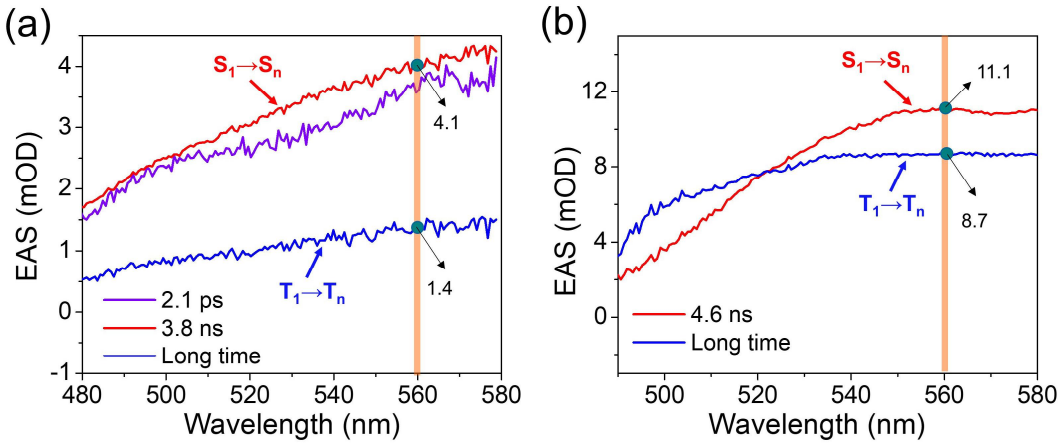

Figure S18. Evolution-associated spectra (EAS) of Ag_{14}-dcbdt in (b) CH_2Cl_2 and (d) the crystalline state were obtained through global fitting of the transient absorption data.

The ratio of ISC ($k_{\mathrm{ISC}}^{\mathrm{crystal}}/k_{\mathrm{ISC}}^{\mathrm{solution}}$) can be roughly estimated through the following equation:

$$I(\mathrm{S}_1 \rightarrow \mathrm{S}_n) = \mathrm{N}(\mathrm{S}_1) \cdot \sigma_S(\mathrm{S}_1 \rightarrow \mathrm{S}_n) \quad (1)$$

$$I(\mathrm{T}_1 \rightarrow \mathrm{T}_n) = \mathrm{N}(\mathrm{T}_1) \cdot \sigma_T(\mathrm{T}_1 \rightarrow \mathrm{T}_n) \quad (2)$$

$$\eta_{\mathrm{ISC}} = \frac{\mathrm{N}(\mathrm{T}_1)}{\mathrm{N}(\mathrm{S}_1)} = \frac{\mathrm{k}_{\mathrm{ISC}}}{\mathrm{k}_{\mathrm{ISC}} + \mathrm{k}_{\mathrm{Fl}} + \mathrm{k}_{\mathrm{nr}}} \quad (3)$$

$$\mathrm{k}_{\mathrm{ISC}} + \mathrm{k}_{\mathrm{Fl}} + \mathrm{k}_{\mathrm{nr}} = \frac{1}{\tau(\mathrm{S}_1)} \quad (4)$$

In which, *I* represents excited state absorption intensity, σ is excited state absorption cross section, N is the number of excitons. k_{ISC}, k_{Fl} and k_{nr} are the rate of intersystem crossing (ISC), prompt fluorescence (Fl) and non-radiative transition, η_{ISC} is the efficiency of ISC. $\tau(S_1)$ is the decay time of singlet excitons. In this work, *I* is the intensity at 560 nm. The $\tau(S_1)$ of Ag_{14}-dcbdt in CH_2Cl_2 and crystalline state are 3.8 ns and 4.6 ns respectively. Assuming that the ratio of σ_S/σ_T does not change with the physical form of the Ag_{14}-dcbdt, the ratio of ISC ($k_{\mathrm{ISC}}^{\mathrm{crystal}}/k_{\mathrm{ISC}}^{\mathrm{solution}}$) was estimated to be 1.9.

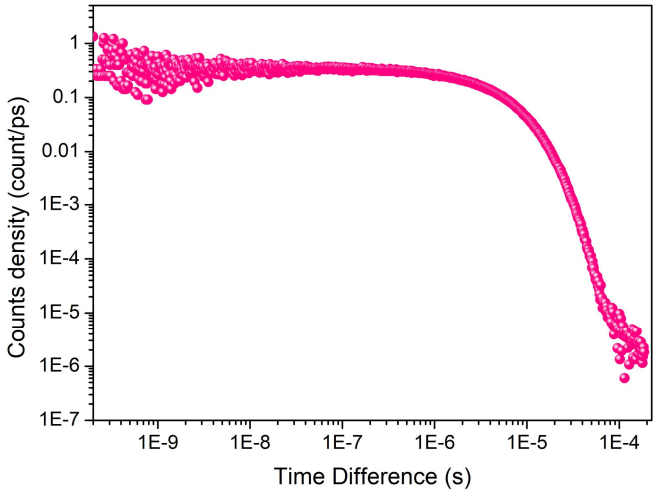

Figure S19. PL decay curves of crystalline samples of Ag_{14}-dcbdt.

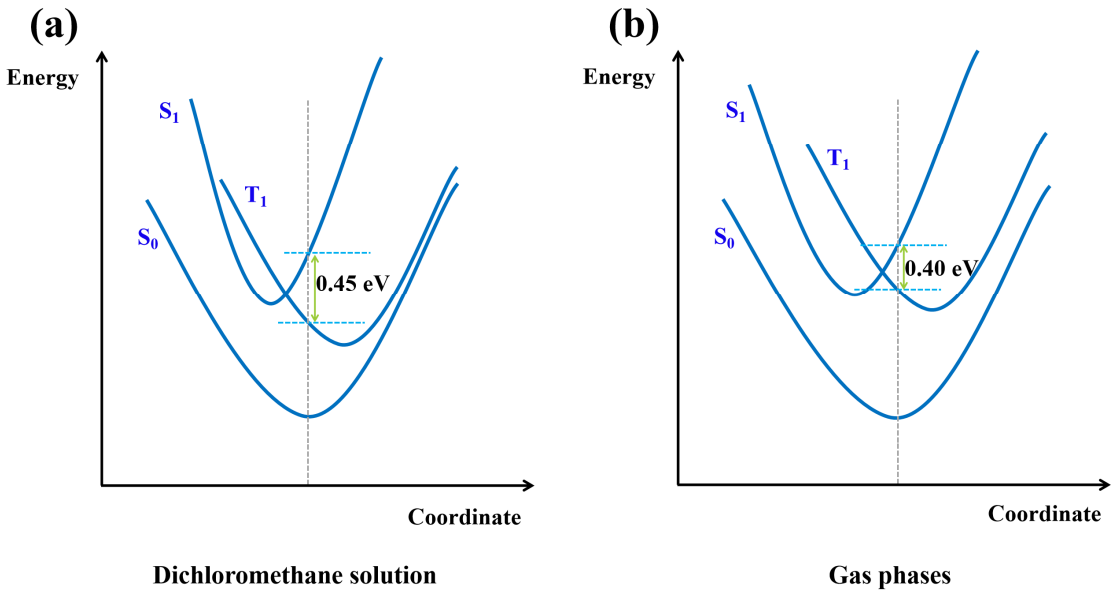

Figure S20 Simulated the energy gap between the S1 and T1states in the dichloromethane solution (a) and gas phase (b).

To qualitatively evaluate the effect of the difference in excited-state energies between solvent and gas phases, we have calculated the ground-state geometry of the molecule in the gas phase. Based on this structure, we simulated the energy gap between the S1 and T1 states. As shown in Fig S20 and Table S3, our results show that the energy gap in the gas phase (0.40 eV) is smaller than that in the dichloromethane solution (0.45 eV). This calculated result is consistent with the experimental trend.

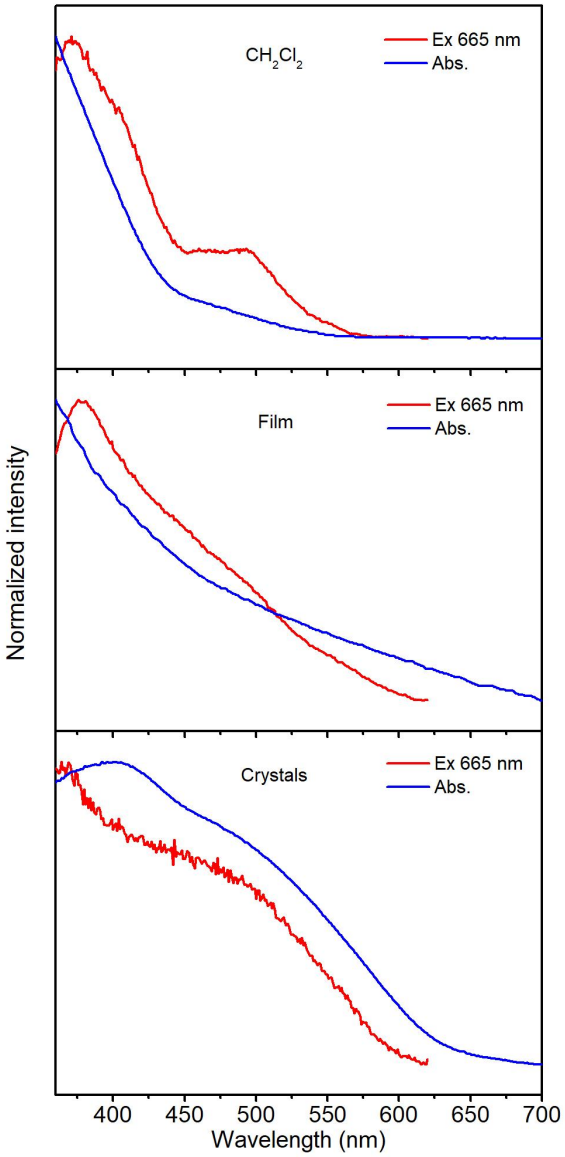

Figure S21. Comparisons of excitation monitoring at 665 nm and absorption/reflectance spectra for Ag_{14}-dcbdt in CH_2Cl_2, PMMA film and in crystalline state.

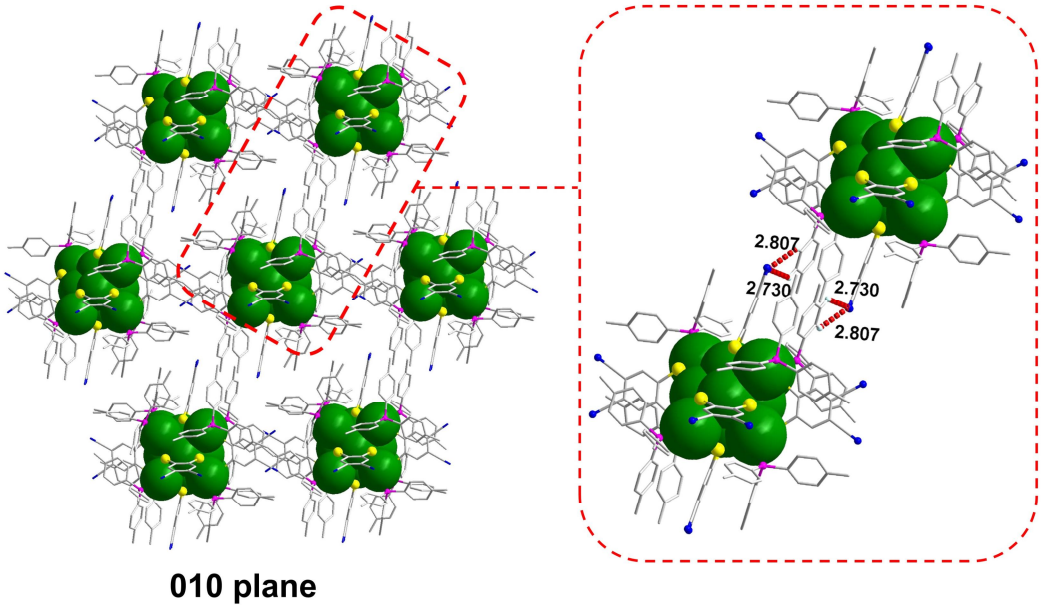

Figure S22. Arrangement of Ag_{14}-dcbdt NCs along the (010) crystal plane and the inter-cluster C–H···N≡C interactions (red dashed line).

Table S1. Crystallographic data and structure refinement for Ag_{14}-dcbdt

	Ag_{14}-dcbdt
CCDC number	2400571
Empirical formula	$C_{216}H_{180}Ag_{14}N_{12}P_8S_{12}$
Formula weight	5086.27
Temperature / K	200
Crystal system	trigonal
Space group	*R*-3
a /Å	20.6758(5)
b /Å	20.6758(5)
c /Å	44.3240(12)
α /°	90
β /°	90
γ /°	120
Volume /Å^3	164109.4(9)
Z	3
ρcalc g/cm^3	1.544
μ /mm^{-1}	11.830
F(000)	7590.0
Crystal size/mm^3	0.050 × 0.050 × 0.050
Radiation	CuKα (λ = 1.54184)
2θ range for data collection /°	5.322 to 147.246
Index ranges	-25 ≤ h ≤ 14, -24 ≤ k ≤ 22, -54 ≤ l ≤ 51
Reflections collected	16452
Independent reflections	7104 [R_{int} = 0.0275, R_{sigma} = 0.0382]
Data/restraints/parameters	7104/42/408
Goodness-of-fit on F2	1.033
Final R indexes [I>=2σ (I)]	R_1 = 0.0801, wR_2 = 0.2241
Final R indexes [all data]	R_1 = 0.0972, wR_2 = 0.2374
Largest diff. peak/hole / e Å^{-3}	1.23/-0.91

Table S2. Transition energy, oscillator strength, and orbital contributions of the strongest electronic excitations of Ag_{14}-dcbdt.

Wavelength (nm)	oscillator strength	Major orbital contributions (≥10%)
319.83	0.4613	H-7 -> L+8 (41.1%), H-8 -> L+6 (15.6%)
397.33	0.2038	H-5 -> L+4 (64.7%)
426.31	0.0357	H -> L (68.7%)

Table S3. The first singlet and triplet excited energies of the Ag_{14}-dcbdt cluster in solution and gas state.

	S_1	T_1	ΔE_{ST}
Dichloromethane	2.9083 eV	2.4578 eV	0.4505 eV
Gaseous state	2.9491 eV	2.5486 eV	0.3997 eV

Supplementary References

1. D. Simão, H. Alves, D. Belo, S. Rabaça, E. Lopes, I. Santos, V. Gama, M. Duarte, R. Henriques, H. Novais and M. Almeida, *Eur. J. Inorg. Chem.,* 2001, 3119-3126.
2. CrysAlisPro 2012, Agilent Technologies. Version 1.171.36.31.
3. G. M. Sheldrick, *Acta Cryst. A* 2015, **71**, 3-8.
4. G. M. Sheldrick, *Acta Cryst. A* 2008, **64**, 112-122.
5. Dolomanov, O. V.; Bourhis, L. J.; Gildea, R. J.; Howard, J. A. K.; Puschmann, *H. J. Appl. Cryst*. 2009, **42**, 339-341.
6. M. J. Frisch, G. W. Trucks, H. B. Schlegel, G. E. Scuseria, M. A. Robb, J. R. Cheeseman, G. Scalmani, V. Barone, G. A. Petersson, H. Nakatsuji, X. Li, M. Caricato, A. V. Marenich, J. Bloino, B. G. Janesko, R. Gomperts, B. Mennucci, H. P. Hratchian, J. V. Ortiz, A. F. Izmaylov, J. L. Sonnenberg, Williams, F. Ding, F. Lipparini, F. Egidi, J. Goings, B. Peng, A. Petrone, T. Henderson, D. Ranasinghe, V. G. Zakrzewski, J. Gao, N. Rega, G. Zheng, W. Liang, M. Hada, M. Ehara, K. Toyota, R. Fukuda, J. Hasegawa, M. Ishida, T. Nakajima, Y. Honda, O. Kitao, H. Nakai, T. Vreven, K. Throssell, J. A. Montgomery Jr., J. E. Peralta, F. Ogliaro, M. J. Bearpark, J. J. Heyd, E. N. Brothers, K. N. Kudin, V. N. Staroverov, T. A. Keith, R. Kobayashi, J. Normand, K. Raghavachari, A. P. Rendell, J. C. Burant, S. S. Iyengar, J. Tomasi, M. Cossi, J. M. Millam, M. Klene, C. Adamo, R. Cammi, J. W. Ochterski, R. L. Martin, K. Morokuma, O. Farkas, J. B. Foresman and D. J. Fox, Journal, 2016.
7. J. P. Perdew, K. Burke, M. Ernzerhof, *Phys. Rev. Lett*. 1996, **77**, 3865-3868.
8. P. C. Hariharan, J. A. Pople, *Theoret. Chimica Acta* 1973, **28**, 213-222.
9. M. M. Francl, W. J. Petro, W. J. Hehre, J. S. Binkley, M. S. Gordon, D. J. DeFrees, J. A. Pople, *J. Chem. Phys*. 1982, **77**, 3654-3665.
10. P. J. Hay, W. R. Wadt, *J. Chem. Phys*. 1985, **82**, 270-283.
11. P. J. Hay, W. R. Wadt, *J. Chem. Phys*. 1985, **82**, 284-298.
12. P. J. Hay, W. R. Wadt, *J. Chem. Phys.* 1985, **82**, 299-310.